IEEE Robotics and Automation Letters (RA-L) paper, presented at ICRA 2023, London, UK. Cite as RA-L paper.

Peg-in-Hole Assembly with Dual-Arm Robot and Dexterous Robot Hands

Dong-Hyuk Lee[1,2], Myoung-Su Choi[1], Hyeonjun Park[3], Ga-Ram Jang[1], Jae-Han Park[1,2] and Ji-Hun Bae[1,2]

***Abstract*—This study focuses on implementing robotic peg-in-hole in a more human-like approach, namely using dual-arms and dexterous robotic hands. The peg-in-hole strategy in this study mainly consists of two parts: grasping strategy (hand part) and assembly strategy (arm part). The grasping strategy explains the fundamental grasping method called "advanced blind grasping" and the in-hand manipulation method that is required for the reorientation of the workpiece. A feed-forward task space force control scheme is proposed for the actual implementation. The assembly strategy presents fundamental unit motions called "perturbation pattern" and proposes four assembly stages that are constructed by a combination of the unit motions. A force-position hybrid control for the implementation of the assembly strategy was also addressed. For evaluation, a peg-in-hole assembly demonstration with a keyhole-like shape was conducted using a human-sized 50-DOF upper-body robot.**

***Index Terms*—peg-in-hole, robot hand, dual-arm robot, assembly automation, force control**

I. Introduction

PEG-IN-HOLE is a type of assembly task that is accomplished by plugging a convex object (referred to as the "peg") into its concave counterpart (referred to as the "hole") of the same shape. Studies on the peg-in-hole problem hold an important position in robotics research because it is a fundamental element towards general assembly capabilities, which are far beyond the current state of technology.

Although the peg-in-hole problem has long been studied in robotics, its importance still makes it an active research area. Recent trends in peg-in-hole studies include passive compliance-based assembly strategies [1], [2], impedance control-based assembly [3], visual-servoing based method [4], and machine learning-based approach [5].

Although numerous studies have been conducted to solve the peg-in-hole problem, previous studies have mostly focused on pure peg-in-hole tasks, in which the peg is fixed to robot arm or held using simple grippers. These approaches reduce the uncertainty of the task and help to focus on the assembly process itself. However, they limit the range for handling the object, which results in less applicability.

Dexterous robot hands have the potential to acquire human-level versatility, which is essential for realizing general assembly capabilities. When it comes to peg-in-hole assembly tasks with dexterous robot hands, very few studies have been published. Shauri et al. introduced a vision based screw and nut assembly technique using three-fingered robot hands and dual-arm robot [6]. Similarly, Koonce et al. reported peg-in-hole insertion using Barrett hand and arm based on proprioceptive information (joint position and torque) [7]. Those works are carried out at a very early stage of research, and the role of hand was not deeply studied. On the other hand, Wyk et al. introduced a fingertip force sensor based peg-in-hole assembly with fine in-hand manipulation technique [8]. The study showed promising results, however, they mainly focused to hand itself, and arm was not deeply involved.

In this study, we attempted the implementation of the whole process of peg-in-hole assembly using a 50-DOF upper-body robot with fully dexterous robot hands, dual arms, and wrists. The main contributions and novelty of this study can be summarized as follows:

$Assembly\ using\ Dexterous\ Robot\ Hands$: The key contribution of this study is the accomplishment of peg-in-hole tasks using dexterous robot hands. This type of robot hands is not optimized for performing a particular task, but it offers the advantage of being able to perform a variety of tasks. In turn, this implies a practical advantage for industrial applications, where the versatility of robot hands can be exploited, e.g., for cell manufacturing without the necessity of tool changing.

$Dual-Arm\ Assembly$: The presence of both arms allows us to conduct various complex tasks that would be difficult with a single arm. In this study, peg-in-hole assembly is performed through the cooperation of both arms, by which one arm serves as a (compliant) fixture holding the hole and the other pushes and aligns the peg to the hole. This procedure is the very similar to how humans perform this task.

$Force\ Control\ and\ Compliant\ Behavior$: From a control perspective, we are particularly interested in human-like quick and adaptive assembly capabilities. In this study, this is achieved by programming a compliant behavior for the robot and employing a feed-forward force-control scheme. This feed-forward force-control scheme results in faster motion in the assembly process owing to the absence of a feedback loop. Compliant behavior allows the robot to naturally cope with contact situations in which external disturbances exist.

The rest of this paper is organized as follows: Section II presents an overview of the whole peg-in-hole procedure

This work was supported in part by Industrial Strategic Technology Development Program (No. 20007058) and in part by the same program (No. 20014558) funded by the Ministry of Trade, Industry & Energy (MOTIE, Korea).

[1]D.-H. Lee, M.-S. Choi, G.-R Jang, J.-H. Park, and J.-H. Bae are with Robotics R&D Department, Korea Institute of Industrial Technology (KITECH), Research Institute of Covergence Technology, Ansan 15588, Korea (e-mail: donghyuk, choims, river.j, hans1024, joseph@kitech.re.kr).

[2]D.-H. Lee, J.-H. Park, and J.-H. Bae are also with Department of Industrial Technology, University of Science and Technology (UST), Daejon 34113, Korea.

[3]H. Park is with ROBROS Co., Anyang 14118, Korea (e-mail: hpark@robros.co.kr)

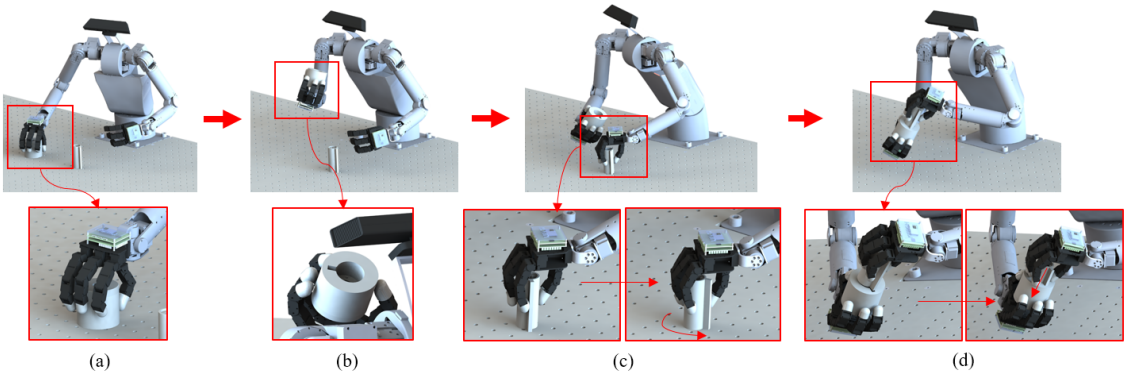

Fig. 1. Overall bimanual peg-in-hole procedure (a) Grasping the hole object. (b) Identifying orientation of the hole. (c) Rotating the peg to match the direction of keyhole. (d) Assembling the peg and hole.

and presents fundamental techniques to achieve it. Sections III and IV present detailed strategies for implementing the elemental techniques from the perspective of using hands and arms, respectively. Finally, the proposed strategies are experimentally verified using a 50-DOF upper-body robot in Section V, and the paper is then concluded.

II. Overall Bimanual Peg-In-Hole Procedure

Fig. 1 shows the whole bimanual assembly process that was implemented in this study. We use keyhole-like-shaped peg and hole objects as shown in the figure. Thus, for them to be properly assembled, their position and orientation should be aligned in all axes. In the initial state, the peg and hole are placed at arbitrary positions on the table. We do not pre-align the peg and hole, and thus there exists an orientation error along the axial direction of the cylinder ranging from 0° to 180°. In this study, it is particularly important to deal with this error. Because the range of motion of the wrist is limited, it is not easy to cover this error solely using wrist motions during assembly. Therefore, it is desirable to make the orientation error be as small as possible before starting the actual assembly maneuvers, which creates the necessity of a few pre-assembly steps.

To this end, we designed a full peg-in-hole process including several pre-assembly steps. The process consists of four major parts: (i) grasping the hole object, (ii) identifying the orientation of the hole, (iii) grasping and reorienting the peg, and (iv) assembling the peg and hole. Fig. 1 shows each part of the process in sequence.

First, the robot identifies the position and orientation of the peg and the position the hole. In this study, a depth camera is used to obtain the position and orientation information of the workpieces. Because the procedure starts with the hole turned upside down, its orientation can only be identified once it has been lifted. Thus, the robot grasps and identifies the orientation of the hole using its left hand, as shown in the first and second steps of Fig. 1.

After obtaining the orientations of the peg and the hole, the robot can calculate the orientation error between them. The robot hands are used to pre-reduce the orientation error, which is very typical of the way in which humans perform peg-in-hole assembly. This error pre-reduction process consists of performing grasping, in-hand rotation, and release actions in series. In-hand rotation is a technique in which one manipulates (rotates) an object using the fingers while grasping it, as shown in the third step of Fig. 1. Depending on the amount of error, this process may be repeated several times owing to the limited range of the in-hand rotation technique. In this study, the error pre-reduction process is called "reorientation" to distinguish it from "in-hand rotation", which is a component of reorientation.

If the orientation error is sufficiently reduced via reorientation, it is possible to proceed to the next assembly step, shown in the fourth step of Fig. 1. The arm grasping the peg (left arm) needs to generate an appropriate force for assembly while the right arm simultaneously regulates the position of the hole. The applied force needs to be properly changed according to the progress of the assembly procedure. A systematic method for generating this force will be discussed in detail in a later section.

III. Grasping Strategy

As previously mentioned, the robot first needs to align the peg and the hole before assembly via reorientation using in-hand rotations. On the other hand, the peg and hole need to be tightly held by the robot hands during the assembly step. In this section, two key techniques for achieving those goals, namely stable grasping and in-hand rotation, are addressed, and control methods for their implementation are presented.

A. Advanced Blind Grasping

We introduce a method called "advanced blind grasping", which is a basic grasping method for this study. Advanced blind grasping was devised to achieve human-like pinch grasping (precision grasping) skills with minimum sensory input and less calculation efforts. The assumptions on the contact model and an earlier form of the method in three-fingers case can be found in [9]. In this study, we present generalization of the previous method in N-fingers case.

Fig. 2 illustrates the basic idea behind advanced blind grasping. The fingertip forces should satisfy the following force and moment equilibrium:

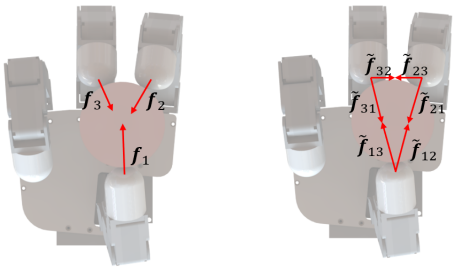

(a) (b)

Fig. 2. Example of advanced blind grasping for $N = 3$. (a) Fingertip forces at equilibrium. (b) Unscaled fingertip force components at equilibrium.

$$\sum_{i=1}^{N} \boldsymbol{f}_i = \boldsymbol{0}, \tag{1}$$

$$\sum_{i=1}^{N} \boldsymbol{p}_i^* \times \boldsymbol{f}_i = \boldsymbol{0}, \tag{2}$$

where $\boldsymbol{p}_i^*$ and $\boldsymbol{f}_i$ represent the position of the fingertip of the i-th finger with respect to an arbitrary point in space and that fingertip's force, respectively. N is the number of fingers participating in the grasping process. Fig. 2(a) represents the fingertip forces at equilibrium when $N = 3$.

Because there exists an infinite number of sets of $\boldsymbol{f}_i$ satisfying the force–moment equilibrium, we need to apply an appropriate constraint to determine a single solution. To this end, we consider the fingertip force $\boldsymbol{f}_i$ as a sum of force components towards other fingertips. Namely,

$$\boldsymbol{f}_i = \sum_{j=1}^{N} \boldsymbol{f}_{ij} \quad (i \neq j), \tag{3}$$

where $\boldsymbol{f}_{ij}$ represents a fingertip force component heading from the i-th fingertip to the j-th fingertip. For example, $\boldsymbol{f}_{12}$ denotes the force component of the thumb's tip force towards the tip of the index finger. In order to calculate each force component, we must first define $\boldsymbol{f}_{ij}$ as follows:

$$\boldsymbol{f}_{ij} = \alpha \tilde{\boldsymbol{f}}_{ij}, \tag{4}$$

where $\tilde{\boldsymbol{f}}_{ij}$ is called the "unscaled fingertip force component", which can be obtained from the kinematic relations between each fingertip. α is a scaling factor that converts the unscaled fingertip force to a physical Cartesian force vector. We define each force component $\tilde{\boldsymbol{f}}_{ij}$ as follows:

$$\tilde{\boldsymbol{f}}_{ij} = \frac{\boldsymbol{p}_j - \boldsymbol{p}_i}{2}, \tag{5}$$

where $\boldsymbol{p}_i$ is the Cartesian position vector of the i-th fingertip. Fig. 2(b) shows force equilibrium conditions expressed using the force components in the case of $N = 3$.

Once we find all fingertip force components using (5), we then need to scale the magnitude of the components to physically meaningful values. This is done via the scaling factor in (4). The scaling factor α is calculated as follows:

$$\alpha = \frac{f_{\text{grasp}}}{\sum_{i=1}^{N} || \sum_{j=1}^{N} \tilde{\boldsymbol{f}}_{ij} ||} \quad (i \neq j), \tag{6}$$

where f_{grasp} is called the net grasping force, which is determined by user. The net grasping force is the sum of the magnitude of all the fingertip forces. Once α is obtained using (6), we can finally determine all the fingertip forces $\boldsymbol{f}_i$ using (3) and (4).

It should be noted that the proposed method does not require knowing the geometry of the grasped object. This makes the method applicable for grasping various objects without any prior knowledge about their shape, and it is the reason why the proposed method was called "blind".

B. Reorientation

Since we are dealing with keyhole-like workpieces, reorientation process should be done in advance of assembling as shown in Fig. 1(c). Reorientation is done by in-hand rotation technique. To this end, we need to break the moment equilibrium described in Eq. 2 while maintaining the force equilibrium by adjusting fingertip forces. The adjusted fingertip force $\boldsymbol{f}_i^*$ of the i-th fingertip is defined as follow:

$$\boldsymbol{f}_i^* = \boldsymbol{f}_i + \boldsymbol{f'}_i, \tag{7}$$

where $\boldsymbol{f}_i$ is the original fingertip force obtained as explained in the previous sub-section and $\boldsymbol{f'}_i$ is the additional fingertip force required to induce the rotation. Fig. 3 presents an example of the additional fingertip force required in the three-finger pinching case.

To calculate $\boldsymbol{f}_i'$, we need to define an axis of rotation first. The axis of rotation is a line defined by a direction vector and a point in the global reference frame. Fig. 3 shows an example of an axis of rotation. The direction vector, $\boldsymbol{z}_{\text{c}}$, is the direction of the axis of rotation, which is given by user. $\boldsymbol{p}_c$ is a point called the "temporal object center", which can be calculated as follows:

$$\boldsymbol{p}_{\text{c}} = \frac{1}{N} \sum_{i=1}^{N} \boldsymbol{p}_i, \tag{8}$$

where $\boldsymbol{p}_i$ is the position of the i-th fingertip. Once the axis of rotation is defined, we can then calculate the additional fingertip force $\boldsymbol{f'}_i$ required at the i-th finger as follows:

$$\boldsymbol{f}_i' = k_{\text{r}}(\theta_{\text{d}} - \theta)(\boldsymbol{z}_{\text{c}} \times \boldsymbol{h}_i), \tag{9}$$

where θ_{d} and k_{r} are the desired rotation angle along the axis of rotation and the rotation gain, respectively. $\boldsymbol{h}_i$ is a perpendicular vector connecting $\boldsymbol{p}_i$ and the axis of rotation, as shown in Fig. 3. $\boldsymbol{h}_i$ can be calculated using known kinematic information as follows:

$$\boldsymbol{h}_i = \boldsymbol{p}_{\text{c}} + \frac{(\boldsymbol{p}_i - \boldsymbol{p}_{\text{c}}) \cdot \boldsymbol{z}_{\text{c}}}{||\boldsymbol{z}_{\text{c}}||^2} \boldsymbol{z}_{\text{c}}. \tag{10}$$

The rotation angle θ in (9) is the current angle of the object along the axis of rotation with respect to its initial pose. More

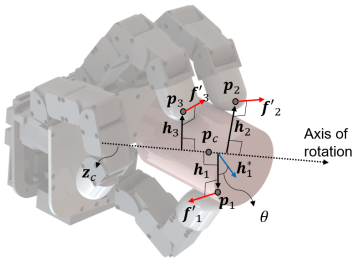

Fig. 3. In-hand rotation method. Note that the axis of rotation does not need to coincide with the geometrical axes of the object.

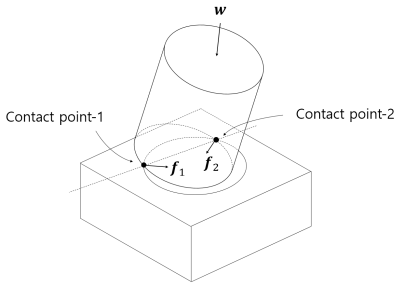

Fig. 4. Qualitative analysis of peg-in-hole assembly. The reaction forces at the contact points naturally guide the peg towards the hole, and the external force helps to overcome the static friction at the contact points.

precisely, in this study, the rotation angle is defined as the angle produced by the "current $\boldsymbol{h}_1$" (expressed as $\boldsymbol{h}_1$) and the "initial $\boldsymbol{h}_1$" (expressed as $\boldsymbol{h}_1^*$) in a plane that contains them both. Fig. 3 shows the rotation angle θ in the three-finger pinching case. The rotation angle can be calculated as follows:

$$\theta = \cos^{-1} \frac{\boldsymbol{h}_1^* \cdot \boldsymbol{h}_1}{||\boldsymbol{h}_1^*||\ ||\boldsymbol{h}_1||}. \tag{11}$$

From the given $\boldsymbol{z}_c$ and the results of (8) and (10)–(11), the additional fingertip force can be calculated using (9). From this equation, it can be easily understood that the additional fingertip forces always satisfy the force equilibrium while breaking the moment equilibrium.

C. Control

Throughout the whole peg-in-hole process, four different types of hand tasks exist, namely (i) shaping, (ii) grasping, (iii) in-hand rotation, (iv) and secure grasping. Shaping refers to tasks done via pure position control, such as pre-shaping (shaping the hand before grasping) or releasing a grasp, which can be achieved through the following control law:

$$\boldsymbol{\tau} = \boldsymbol{J}^{\mathrm{T}} k_{\mathrm{p}} \Delta \boldsymbol{p} + \boldsymbol{\tau}_{\mathrm{g}} + \boldsymbol{\tau}_{\mathrm{f}}, \tag{12}$$

where $\boldsymbol{J} \in \mathbb{R}^{3\times n}$ is the Jacobian matrix of a finger with n degrees of freedom. k_{p} and $\Delta \boldsymbol{p}$ are the proportional gain and the position error vector in Cartesian space for each finger, respectively. $\boldsymbol{\tau}_{\mathrm{g}}$ and $\boldsymbol{\tau}_{\mathrm{f}}$ are gravity and friction compensation vectors, respectively. For grasping, the following feed-forward force-control law is used:

$$\boldsymbol{\tau} = \boldsymbol{J}^{\mathrm{T}} \boldsymbol{f} + \boldsymbol{\tau}_{\mathrm{g}} + \boldsymbol{\tau}_{\mathrm{f}}, \tag{13}$$

where $\boldsymbol{f}$ is the fingertip force obtained as explained in Section III.A. For in-hand rotation, we simply use the tangential force term $\boldsymbol{f}'$ obtained in Section III.B as follows:

$$\boldsymbol{\tau} = \boldsymbol{J}^{\mathrm{T}} (\boldsymbol{f} + \boldsymbol{f}') + \boldsymbol{\tau}_{\mathrm{g}} + \boldsymbol{\tau}_{\mathrm{f}}. \tag{14}$$

Secure grasping is used in the final step of the assembly process to tightly hold the peg and hole objects. In this step, it is important to maintain the position of the fingers tightly against external reaction forces. Basic grasping method in sub-section III.A is not enough for secure grasping since it allows movement of the peg by large external force. There exists several method to resolve this issue. Following is one of simplest method employing feed-forward force control with position regulation:

$$\boldsymbol{\tau} = \boldsymbol{J}^{\mathrm{T}} (k_{\mathrm{p}} \Delta \boldsymbol{p} + \boldsymbol{f}) + \boldsymbol{\tau}_{\mathrm{g}} + \boldsymbol{\tau}_{\mathrm{f}}. \tag{15}$$

IV. Assembly Strategy

A. Analysis on the Peg-in-hole Assembly Process

In this sub-section, we qualitatively analyze the peg-in-hole assembly process and derive its general principles, explaining how assembly can be achieved even in the presence of position uncertainty. Fig. 4 illustrates a situation in which the peg is pushed towards the hole with force $\boldsymbol{w}$. If the compliance of the robot is sufficient, then the peg is slightly tilted, which induces two-point contact, as shown in the figure. Because of the geometry around the contact points, the reaction forces $\boldsymbol{f}_1$ and $\boldsymbol{f}_2$ are generated towards the center of the hole.

It should be noted that the static friction at the contact points prevents the movement of the peg towards the hole if one simply pushes the peg in the normal direction. To overcome this static friction and have the peg be guided by the passive reaction forces, we need to apply an appropriate external force $\boldsymbol{w}$. Because the desirable direction of this external force is unknown, we can simply apply the force in a time-varying arbitrary direction. While this force makes the peg move in arbitrary directions by overcoming the static friction, the passive reaction forces gradually guide the peg towards the hole [10].

In this "guiding" process, the external force can be seen as a perturbation applied to the peg. It is clear that we can make the guiding process finish quickly by choosing a proper pattern for the external force $\boldsymbol{w}$. In this study, this proper pattern for the external force is called the "perturbation pattern". Section IV.B addresses the formulation of this perturbation pattern as a feed-forward force term. In sub-section IV.C, the assembly task is divided into several stages, and a perturbation pattern suitable for each stage is derived.

B. Perturbation Patterns

We now define basic perturbation patterns, which will be used as building blocks for each stage of the assembly process. Fig. 5 shows the four basic perturbation patterns

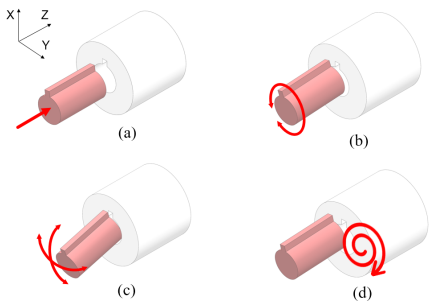

Fig. 5. Basic perturbation patterns: (a) Pushing, (b) Rubbing, (c) Wiggling, and (d) Spiral motion

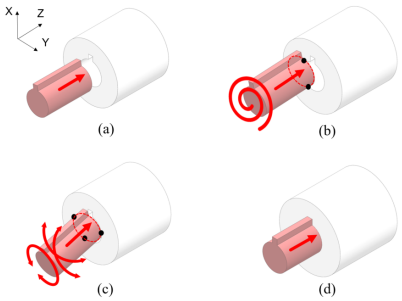

Fig. 6. Assembly stages for a keyhole-like peg and hole (Note that each stage is constructed by combining unit motions in Fig.8). (a) Approaching, (b) Searching (two-point contact), (c) Aligning (three-point contact), and (d) Inserting.

used in this study. Each perturbation pattern is expressed as a wrench vector that varies over time. First, we define a general perturbation $\boldsymbol{w}$ as follows:

$$\boldsymbol{w} = [w_1 \ w_2 \ w_3 \ w_4 \ w_5 \ w_6]^{\mathrm{T}}, \tag{16}$$

where $[w_1, w_2, w_3]$ and $[w_4, w_5, w_6]$ are the translation and rotation force components in the x, y, and z-axes, respectively. Each force component is expressed in the time domain as follows:

$$w_i = a_i \sin(b_i t + c_i) + d_i, \quad i \in \{1, 2, ...6\}, \tag{17}$$

which can be rewritten in vector form as follows:

$$\boldsymbol{w} = \mathrm{diag}(\boldsymbol{a}) \ \mathrm{vsin}(t\boldsymbol{b} + \boldsymbol{c}) + \boldsymbol{d}, \tag{18}$$

where $\boldsymbol{a}, \boldsymbol{b}, \boldsymbol{c}$, and $\boldsymbol{d} \in \mathbb{R}^{6\times 1}$ are parameters of the perturbation wrench vector. $\mathrm{vsin}(\boldsymbol{x})$ is a vectorized version of the sine function maps $x \in \boldsymbol{x}$ to $\sin(x)$.

Each perturbation pattern used in this research is defined by a set of perturbation parameters. A pushing motion along the z-axis, as shown in Fig. 5(a), can be simply generated via the perturbation patter $\boldsymbol{w}_{\mathrm{push}}$ produced by the following parameter set:

$$\begin{aligned} \boldsymbol{a} &= \boldsymbol{b} = \boldsymbol{c} = \boldsymbol{0}^{\mathrm{T}}, \\ \boldsymbol{d} &= [\ 0 \ 0 \ f_{\mathrm{push}} \ 0 \ 0 \ 0 \ ]^{\mathrm{T}}. \end{aligned} \tag{19}$$

A rubbing motion around the z-axis, as shown in Fig. 5(b), can be generated via the perturbation pattern $\boldsymbol{w}_{\mathrm{rub}}$ produced by the following parameter set:

$$\begin{aligned} \boldsymbol{a} &= [\ 0 \ 0 \ 0 \ 0 \ 0 \ f_{\mathrm{rub}} \ ]^{\mathrm{T}}, \\ \boldsymbol{b} &= [\ 0 \ 0 \ 0 \ 0 \ 0 \ v_{\mathrm{rub}} \ ]^{\mathrm{T}}, \\ \boldsymbol{c} &= \boldsymbol{d} = \boldsymbol{0}^{\mathrm{T}}. \end{aligned} \tag{20}$$

A wiggling motion around the x and y axes, as shown in Fig. 5(c), can be generated via the perturbation pattern $\boldsymbol{w}_{\mathrm{wiggle}}$ produced by the following parameter set:

$$\begin{aligned} \boldsymbol{a} &= [\ 0 \ 0 \ 0 \ f_{\mathrm{wiggle}} \ f_{\mathrm{wiggle}} \ 0 \ ]^{\mathrm{T}}, \\ \boldsymbol{b} &= [\ 0 \ 0 \ 0 \ v_{\mathrm{wiggle}} \ v_{\mathrm{wiggle}} \ 0 \ ]^{\mathrm{T}}, \\ \boldsymbol{c} &= [\ 0 \ 0 \ 0 \ 0 \ \pi/2 \ 0 \ ]^{\mathrm{T}}, \\ \boldsymbol{d} &= \boldsymbol{0}^{\mathrm{T}}. \end{aligned} \tag{21}$$

A spiral motion in the $x-y$ plane, as shown in Fig. 5(d), can be generated via the perturbation pattern $\boldsymbol{w}_{\mathrm{spiral}}$ produced by the following parameter set:

$$\begin{aligned} \boldsymbol{a} &= [\ f_{\mathrm{spiral}}(t) \ f_{\mathrm{spiral}}(t) \ 0 \ 0 \ 0 \ 0 \ ]^{\mathrm{T}}, \\ \boldsymbol{b} &= [\ v_{\mathrm{spiral}} \ v_{\mathrm{spiral}} \ 0 \ 0, 0 \ 0 \ ]^{\mathrm{T}}, \\ \boldsymbol{c} &= [\ 0 \ \pi/2 \ 0 \ 0 \ 0 \ 0 \ ]^{\mathrm{T}}, \\ \boldsymbol{d} &= \boldsymbol{0}^{\mathrm{T}}, \\ f_{\mathrm{spiral}}(t) &= \alpha \sin(v_{\mathrm{spiral}} t) + \beta. \end{aligned} \tag{22}$$

In (19)–(22), f_{pattern} and v_{pattern} are the force magnitude and frequency coefficients for each pattern, respectively. α and β in (22) are the variation and mean force magnitude for the spiral force, respectively.

C. Assembly Stages

Peg-in-hole assembly (excluding the pre-assembly steps) consists of several stages that need to be dealt with differently. In this study, we define four different assembly stages and propose an appropriate perturbation pattern for each stage.

Fig. 6 shows the assembly stages. The first stage is "approaching", in which the peg approaches the hole while both face each other with some amount of uncertainty. Because there is no contact, pushing is enough to produce the approaching perturbation:

$$\boldsymbol{w}_{\mathrm{approach}} = \boldsymbol{w}_{\mathrm{push}}. \tag{23}$$

Once the peg and the hole are in contact with each other, the peg is then slightly tilted by the compliance of the robot and two-point contact occurs, as shown in Fig. 6(b). This is called the "searching" stage because the robot needs to search for the hole at this point. In this stage, the peg is movable on the x–y plane along the edge of the hole, and thus we can employ the spiral pattern to search for the hole. The searching stage can be implemented as a combination of spiral and pushing patterns using (19) and (22), namely:

$$\boldsymbol{w}_{\mathrm{search}} = \boldsymbol{w}_{\mathrm{push}} + \boldsymbol{w}_{\mathrm{spiral}}. \tag{24}$$

During the searching phase, the peg may get stuck around the entrance to the hole. In this stage, three-point contact occurs, as shown in Fig. 6(c). This is called the "aligning" stage because it is necessary to align the orientation of the peg

and hole at this point. The aligning stage can be implemented as a combination of rubbing, wiggling, and pushing patterns using (19), (21), and (20), namely:

$$\boldsymbol{w}_{\text{align}} = \boldsymbol{w}_{\text{push}} + \boldsymbol{w}_{\text{wiggle}} + \boldsymbol{w}_{\text{rub}}. \tag{25}$$

Once aligning is successfully done, the peg can be inserted through the hole as shown in Fig. 6(d). This is called the "inserting" stage. The inserting stage is basically the same as the approaching stage as follow:

$$\boldsymbol{w}_{\text{insert}} = \boldsymbol{w}_{\text{push}}. \tag{26}$$

D. Control

Since we use a dual-arm robot to handle the peg and hole, special consideration should be conducted. During the assembly process, the arm holding the hole (left arm in this paper) should tightly regulate its position against external forces, i.e., perturbation wrenches. In this case conventional position control with medium or high gain is suitable option. In this study, a task space position control law in (15) with medium position gain, $500 \leq k_p \leq 1000$, is used for this purpose.

On the other hand, the arm holding the peg (right hand in this paper) should generate the perturbation wrench while maintaining the peg's position. For this reason, the right arm is controlled in a hybrid force–position control fashion as follows:

$$\begin{aligned}\boldsymbol{\tau} = \boldsymbol{J}^{\mathrm{T}} \begin{bmatrix} \boldsymbol{\Omega} & \boldsymbol{0} \\ \boldsymbol{0} & \boldsymbol{I} \end{bmatrix} \boldsymbol{K}_{\mathrm{p}} \Delta \boldsymbol{x} + \boldsymbol{J}^{\mathrm{T}} \begin{bmatrix} \boldsymbol{R}_{\mathrm{h}} & \boldsymbol{0} \\ \boldsymbol{0} & \boldsymbol{R}_{\mathrm{h}} \end{bmatrix} \boldsymbol{w} \\ - \boldsymbol{D}\dot{\boldsymbol{q}} + \boldsymbol{\tau}_{\mathrm{g}} + \boldsymbol{\tau}_{\mathrm{f}}.\end{aligned} \tag{27}$$

The first and second terms in (27) play the roles of position and force control, respectively. The first term generates the joint torque for regulating the desired task-space position excluding the axis in which the pushing force is applied. This is done via a generalized task specification matrix $\boldsymbol{\Omega} \in \mathbb{R}^{3\times3}$, which can be expressed as follows [11]:

$$\boldsymbol{\Omega} = \boldsymbol{R}_{\mathrm{h}} \Sigma \boldsymbol{R}_{\mathrm{h}}^{\mathrm{T}}, \tag{28}$$

where $\boldsymbol{\Sigma}$ is a selection matrix that chooses an axis in which position should be controlled. In this study, we always set the axis along which the pushing force is applied as x, and thus $\boldsymbol{\Sigma} = \mathrm{diag}([0\ 1\ 1])$. $\boldsymbol{R}_{\mathrm{h}}$ is the rotation matrix of the hole with respect to the global reference frame. $\boldsymbol{K}_{\mathrm{p}}$ and $\Delta\boldsymbol{x}$ are the proportional gain matrix and the position error vector, respectively. Herein the proportional gain needs to be low to provide sufficient compliance during assembly. Low proportional gain also enables slight motion to arise due to the perturbation wrench.

The second term in (27) transforms the perturbation wrench $\boldsymbol{w}$ with respect to the global reference frame and produces joint torque via $\boldsymbol{J} \in \mathbb{R}^{6\times n}$, which is the Jacobian matrix of the robot arm with n degrees of freedom. It should be noted the perturbation wrench is given by user according to the assembly stage and there is no force feedback term.

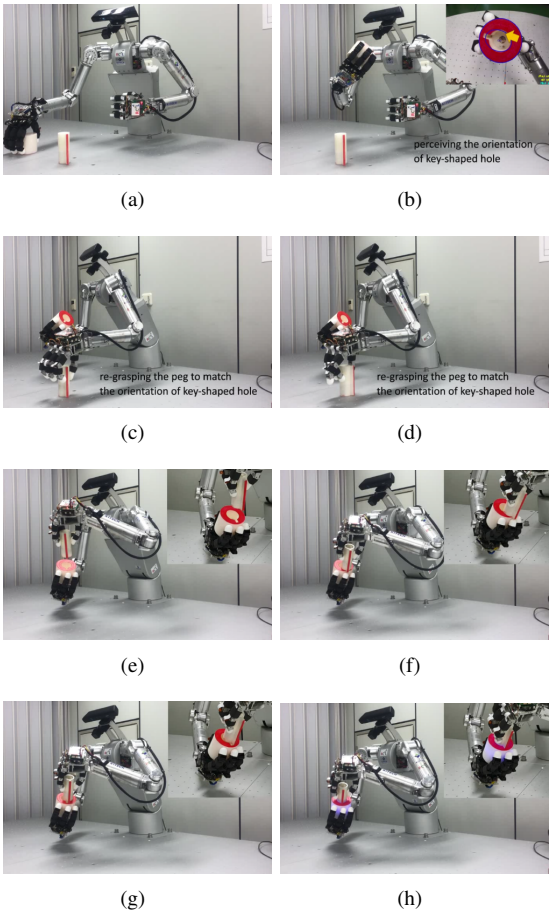

(a) (b) (c) (d) (e) (f) (g) (h)

Fig. 7. Entire bimanual peg-in-hole experiment. (a)–(b) Identifying the axial angle of the hole. (c)–(d) Reorienting the peg. (e) Approaching stage. (f) Searching stage. (g) Aligning stage. (h) Completion of insertion.

The third term is used when $n > 6$ and the joint's friction is particularly low in order to prevent null motion due to redundancy. $\boldsymbol{D}$ and $\dot{\boldsymbol{q}}$ represent a damping matrix and joint space velocity, respectively. An appropriate damping matrix can be obtained from the inertia matrix of the robot [12]. Finally, $\boldsymbol{\tau}_{\mathrm{g}}$ and $\boldsymbol{\tau}_{\mathrm{f}}$ are gravity and the joint friction-compensation vector, respectively.

V. Experiments

A. Experimental Environment

For the experimental verification of the proposed strategies, a 50-DOF upper-body robot was used. The robot consists of an 18-DOF upper body (without hands) and two 16-DOF robot hands. Each robot hand consists of four 4-DOF torque-controllable fingers that provide sufficient dexterity to implement the proposed grasping strategy [13]. The upper body includes two biologically inspired 8-DOF arms and a 2-DOF waist with fully torque-controllable joints [14]. The upper body and the hands are independently controlled.

For the identification of the position and orientation of the objects, an RGBD sensor (Microsoft KINECT) was mounted on top of the robot. The spatial position and orientation of the peg and hole are estimated using 3D depth information and 2D RGB pictures, respectively.

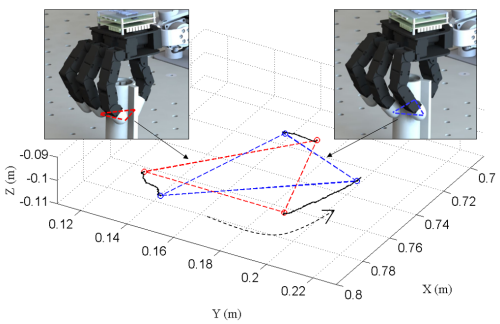

(a)

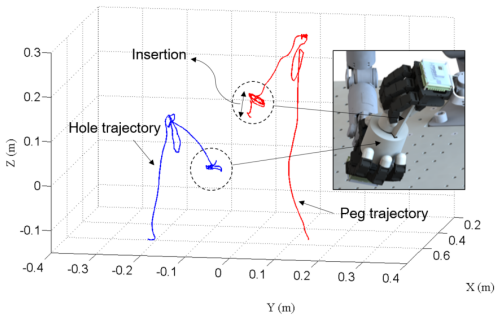

(b)

Fig. 8. Assembly sub-task results. (a) Reorientation. (b) Trajectories of the peg and hole during assembly (excluding pre-assembly steps).

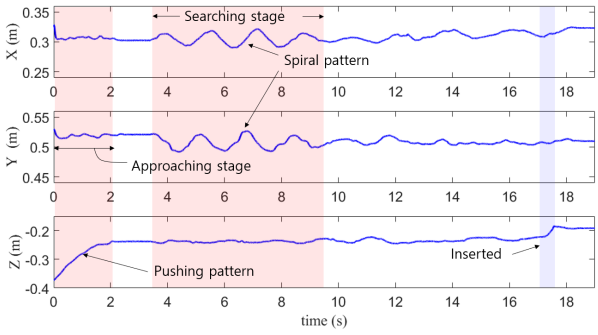

(a)

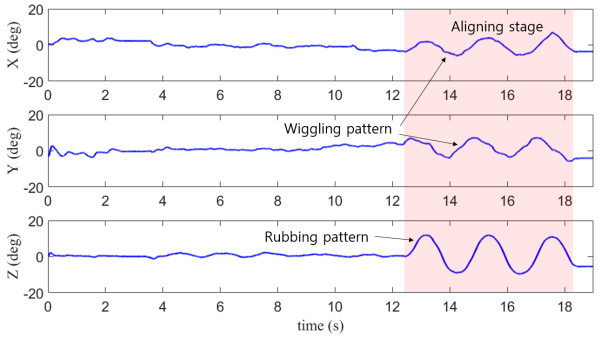

(b)

Fig. 9. Time-domain trajectory of the peg during the assembly. (a) Position. (b) Orientation.

The peg and hole used in our experiments were fabricated using a 3D printer, and the clearance at the circular part was 0.5 mm. For easier identification via the RGBD sensor, a side of the peg and the top surface of the hole were colored red, as shown in Fig. 7.

B. Experiment: Whole Process

Fig. 7 shows the entire experimental procedure for bimanual peg-in-hole assembly conducted in this study. First, the positions of the peg and the hole and the orientation of the hole are obtained using the RGBD sensor. Then, the robot grasps and lifts the hole and identifies its axial angle, as shown in Fig. 7(a) and Fig.7(b). Subsequently, the robot reorients the peg on the table by repeating the "grasping, in-hand rotation, and releasing" sequence twice (Fig. 7(c) and Fig. 7(d)). After that, the assembly task is conducted in the aforementioned sequence of approaching (Fig. 7(e)), searching (Fig. 7(f)), aligning (Fig. 7(g)), and inserting (Fig. 7(h)). The total time required to accomplish the whole procedure was 52 s.

Fig. 8(a) shows the zoomed-in trajectory of the fingertips during the reorientation process (Fig. 7(c) and Fig. 7(d)). The vertices of the triangles in the figure indicate the position of the fingertips during rotation. From the measured trajectory, the rotation of the peg was clearly confirmed. Reorientation was performed twice in the same manner, but only one result was shown to avoid duplication. Fig. 8(b) shows the spatial trajectories of the peg (red line) and the hole (blue line) during the assembly maneuver (Fig. 7(e)–Fig. 7(h)). The spiral motion and the insertion of the peg can be clearly identified from the measured trajectories.

Each of the assembly stages, namely approaching, searching, and aligning, can be more clearly observed in the time-domain trajectory of the peg shown in Fig. 9. Fig. 9(a) shows the position of the peg, which was calculated using the fingertip triangle (thumb, index, and middle fingers). Fig. 9(b) shows the orientation of the end effector of the left arm, which can be approximately assumed to be the orientation of the peg.

The approaching and searching stages can be observed in Fig. 9(a) in the form of pushing and spiral patterns, respectively. The aligning stage can be identified in Fig. 9(b) in the form of wiggling and rubbing patterns. The insertion of the peg can be identified from the sudden increase in the z-axial position of the peg, as shown in Fig. 9(a). As previously mentioned in sub-section III.C, due to the sudden insertion of the peg during aligning, there was no explicit insertion stage in this experiment. It can be seen the wiggling and rubbing patterns lasted for a short additional time after the completion of the insertion. In this experiment, transitions between the stages were manually controlled.

C. Experiment: Assembling Scenarios

Basically, the assembly process consists of four stages - approaching, searching, aligning and inserting. However, in many cases, some of these stages can be omitted. For example, if a three-point contact state is created by chance after approaching, the searching stage is unnecessary. For this reason, four different assembly scenarios(cases) are possible. Fig. 10 illustrates the possible four assembly cases. Through intensive assembly experiments, we confirmed the frequency and

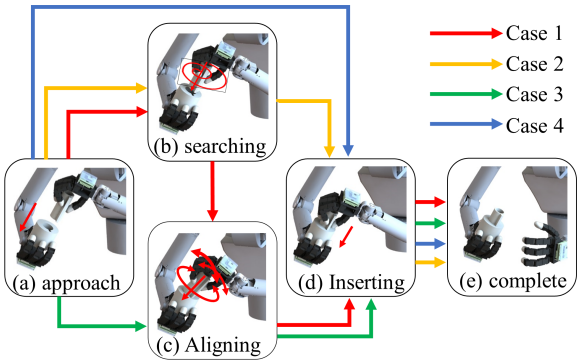

Fig. 10. Four possible peg-in-hole assembly scenarios.

TABLE I
STATISTICAL RESULTS OF REPETITIVE ASSEMBLY EXPERIEMENTS

Case number	Success Count (success/trial)	Average time
Case 1	33	19.42 [s]
Case 2	41	11.87 [s]
Case 3	5	10.20 [s]
Case 4	8	3.37 [s]
Total	87/100	13.86 [s]

success rate of each case. Table I shows experimental results obtained after 100 repetitive experiments. Case 1, the full scenario including approaching, searching, aligning and inserting stages, took longest average assembly time (19.42 s) with 33 successes. Case 2 (approaching-searching-inserting) was most frequently observed (41 successes), and case 3 (approaching-aligning-inserting) ware rarest (5 successes). Case 4 showed shortest average assembly time (3.37 s) with 8 successes due to the absence of searching and aligning stages. Fig. 11 depicts trajectory of the peg and hole in each representative case. Total success rate was 87% and total average assembly time was 13.86 s. In the experiments, transition between the stages were manually controlled based on the observation of the human operator. Fully autonomous stage transition will be our next research topic.

VI. CONCLUSIONS

In this paper, strategies and implementation results for robotic peg-in-hole assembly with a dual-arm robot and dexterous robot hands were presented. Two core techniques, namely a grasping strategy for the robot hands and an assembly strategy for the robot arms, were thoroughly addressed. For the grasping strategy, stable object grasping and an in-hand object-rotation technique based on a feed-forward force term were introduced. For the assembly strategy, the concept of perturbation was introduced as a key to accomplish the assembly tasks, and several perturbation patterns appropriate for each of the approaching, searching, aligning, and inserting stages of the peg-in-hole task were designed in the form of feed-forward force terms. Finally, the whole bimanual peg-in-hole assembly process was implemented using a 50-DOF upper-body robot. Armed with the presented core techniques, the whole assembly process was successfully demonstrated and statistical experimental results were obtained with 87% success rate.

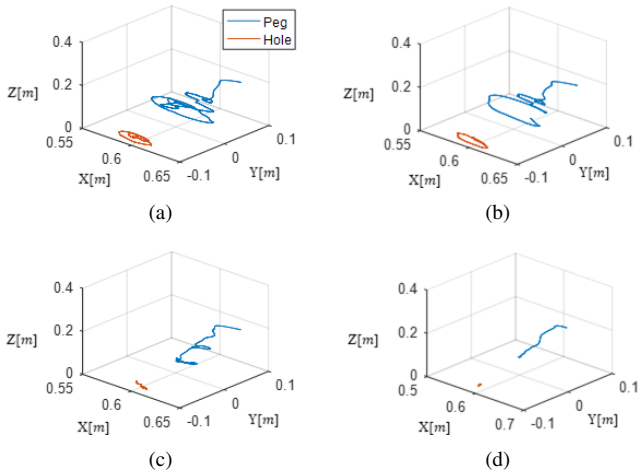

Fig. 11. Trajectory of peg and hole during assembly in four different cases. (a) Case 1. (b) Case 2. (c) Case 3. (d) Case 4.

REFERENCES

[1] H. Park, J. Park, D.-H. Lee, J.-H. Park, M.-H. Baeg, and J.-H. Bae, "Compliance-based robotic peg-in-hole assembly strategy without force feedback," *IEEE Trans. Ind. Electron.*, vol. 64, no. 8, pp. 6299–6309, 2017.

[2] X. Li, R. Li, H. Qiao, C. Ma, and L. Li, "Human-inspired compliant strategy for peg-in-hole assembly using environmental constraint and coarse force information," in *IEEE/RSJ Int. Conf. Intell. Robots Syst.*, pp. 4743–4748. IEEE, 2017.

[3] H.-C. Song, Y.-L. Kim, and J.-B. Song, "Guidance algorithm for complex-shape peg-in-hole strategy based on geometrical information and force control," *Adv. Robot.*, vol. 30, no. 8, pp. 552–563, 2016.

[4] W. Gao and R. Tedrake, "kpam 2.0: Feedback control for category-level robotic manipulation," *IEEE Robot. Autom. Letters*, vol. 6, no. 2, pp. 2962–2969, 2021.

[5] S. A. Khader, H. Yin, P. Falco, and D. Kragic, "Stability-guaranteed reinforcement learning for contact-rich manipulation," *IEEE Robot. Autom. Letters*, vol. 6, no. 1, pp. 1–8, 2020.

[6] R. L. A. Shauri and K. Nonami, "Assembly manipulation of small objects by dual-arm manipulator," *Assem. Autom.*, 2011.

[7] P. Koonce, V. Dutell, J. Farrington, V. Sukhoy, and A. Stoytchev, "Toward learning to solve insertion tasks: A developmental approach using exploratory behaviors and proprioception," in *AAAI Conf. Artif. Intell.*, 2011.

[8] K. Van Wyk, M. Culleton, J. Falco, and K. Kelly, "Comparative peg-in-hole testing of a force-based manipulation controlled robotic hand," *IEEE Trans. Robot.*, vol. 34, no. 2, pp. 542–549, 2018.

[9] J.-H. Bae, S.-W. Park, D. Kim, M.-H. Baeg, and S.-R. Oh, "A grasp strategy with the geometric centroid of a groped object shape derived from contact spots," in *IEEE Int. Conf. Robot. Autom.*, pp. 3798–3804. IEEE, 2012.

[10] M. A. Peshkin, "Programmed compliance for error corrective assembly," *IEEE Trans. Robot. Autom.*, vol. 6, no. 4, pp. 473–482, 1990.

[11] O. Khatib, "A unified approach for motion and force control of robot manipulators: The operational space formulation," *IEEE J. Robot. Autom.*, vol. 3, no. 1, pp. 43–53, 1987.

[12] S. Arimoto, M. Sekimoto, H. Hashiguchi, and R. Ozawa, "Natural resolution of ill-posedness of inverse kinematics for redundant robots: A challenge to bernstein's degrees-of-freedom problem," *Adv. Robot.*, vol. 19, no. 4, pp. 401–434, 2005.

[13] D.-H. Lee, J.-H. Park, S.-W. Park, M.-H. Baeg, and J.-H. Bae, "Kitech-hand: A highly dexterous and modularized robotic hand," *IEEE/ASME Trans. Mechatronics*, vol. 22, no. 2, pp. 876–887, 2016.

[14] D.-H. Lee, H. Park, J.-H. Park, M.-H. Baeg, and J.-H. Bae, "Design of an anthropomorphic dual-arm robot with biologically inspired 8-dof arms," *Intell. Serv. Robot.*, vol. 10, no. 2, pp. 137–148, 2017.